

# Experimental Method to Constrain Preferential Emission and Spectator Dynamics in Heavy-Ion Collisions

Vipul Bairathi<sup>a</sup>, Somadutta Bhatta<sup>b,\*</sup>

<sup>a</sup>*Instituto de Alta Investigación, Universidad de Tarapacá, Casilla 7D, Arica, 1000000, Chile*

<sup>b</sup>*Department of Chemistry, Stony Brook University, Stony Brook, 11974, New York, USA*

---

## Abstract

We introduce a novel experimental method to quantify contribution of preferential emission to the pseudorapidity distribution of produced particles in heavy-ion collisions using correlations between spectator asymmetry and final-state multiplicity. Within a transport model, the magnitude of this correlator increases from mid to forward rapidities, reflecting the impact of preferential emission and capturing fluctuations in sources of particle production. The correlator demonstrates sensitivity to spectator number fluctuations arising from evaporation or fragmentation, providing a handle to constrain such dynamics. This method serves as a powerful tool to probe particle production mechanisms and the space-time evolution of spectator matter in heavy-ion collisions.

*Keywords:* Pseudorapidity distribution, Preferential Emission, Spectator Fragmentation

*PACS:* 25.75.Dw, 25.75.Gz

---

## 1. Introduction

Understanding the mechanisms of particle production is one of the primary goals in high-energy heavy-ion collisions. One of the key aspect of these mechanisms is related to the dynamics governing the pseudorapidity ( $\eta$ ) distribution of particles, which is crucial for constraining the three-dimensional energy density profile in the initial state [1, 2, 3, 4, 5]. Significant strides in this direction have been made through experimental measurements and phenomenological investigations into forward-backward multiplicity correlations, flow-decorrelations, and baryon stopping [6, 7, 8, 9, 10, 11, 12].

In QCD-inspired string models, particle production occurs through string formation, where the number of strings is equal to the number of participant nucleons ( $N_{\text{part}}$ ) [13, 14]. Color-neutral hadrons are subsequently produced through string fragmentation. Event-by-event fluctuations in string lengths and endpoints lead to variations in the longitudinal distribution of produced particles,  $P(\eta)$  [14, 15, 16, 17]. Previous studies of forward-backward multiplicity correlations and  $P(\eta)$  in asymmetric collision systems suggest that nucleons emit more particles in the direction of their motion, with forward (backward) moving nucleons emitting more particles in forward (backward)  $\eta$  [12, 18, 19, 20]. This behavior, known as preferential emission, coupled with the forward-backward asymmetry in  $N_{\text{part}}$ , leads to event-by-event asymmetries in  $P(\eta)$  and drives the observed long-range multiplicity correlations in  $\eta$  [10]. Moreover, the preferential emission mechanism is crucial for explaining experimentally measured longitudinal flow-decorrelations and directed-flow [6, 21, 22, 23, 24]. Therefore, developing novel experimental observables that quantify the correlation between the forward-backward asymmetry of  $N_{\text{part}}$  and multiplicity is crucial to provide stronger constraints on the mechanism of preferential emission.

However, direct measurement of  $N_{\text{part}}$  in heavy-ion collision experiments is not feasible. Instead, neutron and proton spectators, which provide indirect information about  $N_{\text{part}}$ , can be detected using Zero-Degree Calorimeters (ZDC) and forward proton detectors, such as Atlas Forward Proton (AFP) detector [25, 26, 27, 28]. But again, not

---

\*Corresponding Author

*Email address:* somadutta.bhatta@stonybrook.edu (Somadutta Bhatta)

all spectators are detected experimentally due to dynamic processes such as fragmentation and evaporation. The Abrasion-Ablation model [29, 30] describes this process: participant nucleons are sheared from the colliding nuclei (Abrasion), exciting the spectator fragment, which then de-excites through multi-fragmentation or evaporation (Ablation). These processes result in charged fragments that deviate from the expected trajectories of individual spectator nucleons in the beam direction, primarily due to differences in their charge-to-mass ratios. This deviation reduces the number of spectators detected in ZDC and AFP.

Moreover, the charged fragments produced from aforementioned spectator dynamics are deposited in a wide range of  $\eta$ , centered around beam-rapidity,  $y_{\text{beam}}$  [31, 32]. Experimental measurements have shown that the contribution of spectator dynamics to the measured  $P(\eta)$  increases with decreasing collision energy and as collisions become more peripheral[33]. Therefore, for reliable measurements of observables sensitive to number of charged particles in relatively forward-rapidities, it is essential to quantify the contributions from spectator dynamics, particularly at lower collision energies. Additionally, the separation of spectators from colliding nuclei involves energy exchanges between nucleons, and the subsequent dynamics are influenced by nuclear energy levels. Understanding this process is crucial for elucidating fundamental aspects of nucleon emission mechanisms and the Equation of State (EoS) of nuclear matter [34, 35, 36, 37].

Currently, experimental measurements rely on model comparisons to evaluate the contribution of  $N_{\text{part}}$  asymmetry to long-range multiplicity correlations. To quantify this contribution, a novel observable that correlates  $N_{\text{part}}$  asymmetry with final-state multiplicity asymmetry is proposed in this letter. Furthermore, spectator dynamics are expected to influence the particle distribution near mid-rapidity, particularly at lower collision energies [31, 38]. However, these processes are not adequately modeled in the current frameworks used to simulate heavy-ion collisions. The proposed correlator addresses this issue by providing a method to quantify the fluctuations in number of spectators due to fragmentation and evaporation in experimental measurements, thereby providing strong constraints for modeling these dynamics.

## 2. Method

In heavy-ion collisions, nucleons that undergo collisions are called ‘‘participants’’, while those moving along the beam direction without interacting are called ‘‘spectators’’. The total  $N_{\text{part}}$  is the sum of forward ( $N_{\text{part,F}}$ ) and backward ( $N_{\text{part,B}}$ ) moving participants, which fluctuate event-by-event due to quantum mechanical effects. Previous studies [39, 40] indicate that the initial asymmetry between  $N_{\text{part,F}}$  and  $N_{\text{part,B}}$  in an event contributes asymmetrically to  $P(\eta)$  around  $\eta = 0$  [18, 21, 41, 42, 43]. The contribution of this asymmetry can be quantified by correlating the forward-backward asymmetry of participants in the initial state with the forward-backward asymmetry of produced particles in the final state on an event-by-event basis.

Studies on preferential emission has been typically carried out within models that include the fragmentation of wounded nucleons [12, 18, 19, 20]. Similar features have also been reported within A Multi-Phase Transport (AMPT) model where the initial conditions after the collisions are modeled using HIJING [14, 10, 44]. The AMPT model, widely used to simulate the space-time evolution of matter formed in heavy-ion collisions, provides a good description of experimentally measured collective flow and particle spectra [45, 46, 47, 48, 49, 50, 51, 52]. Therefore, this study employs the AMPT model to investigate preferential emission in Au+Au collisions simulated at  $\sqrt{s_{NN}} = 200$  GeV. The total number of pions, kaons, and protons with transverse momentum,  $p_T < 10$  GeV constitutes the multiplicity ( $N_{\text{ch}}$ ) in an event. Centrality is determined by dividing the distribution of  $N_{\text{ch}}$  within  $|\eta| < 0.2$  into percentiles, where centrality of 0% corresponds to the most central collisions with largest  $N_{\text{ch}}$ . All observables in this study are calculated for  $|\eta| > 0.2$  to avoid any overlap between the  $N_{\text{ch}}$  used for determining centrality and those used for calculating the observables.

We begin with the general idea that  $P(\eta)$  has contributions from both rapidity-odd and rapidity-even sources of particle production, with the rapidity-even components contributing symmetrically about  $\eta = 0$  [18, 21, 41, 42, 43]. The forward-backward multiplicity asymmetry in each event is defined as:  $A_{\text{ch},\eta} = N_{\text{ch},\eta} - N_{\text{ch},-\eta}$ , where  $N_{\text{ch},\eta}$  is the number of charged particles within a narrow interval  $\delta\eta$ , centered at  $\eta$ . The  $A_{\text{ch},\eta}$  is an odd function of  $\eta$ , as  $A_{\text{ch},\eta} = -A_{\text{ch},-\eta}$ . Similarly, the participant asymmetry in each event is defined as:  $A_{\text{part}} = N_{\text{part,F}} - N_{\text{part,B}}$ . The number of forward-going spectators,  $N_{\text{spec,F}}$  is anti-correlated to  $N_{\text{part,F}}$ , as  $N_{\text{spec,F}} = A - N_{\text{part,F}}$ , where  $A$  is the mass number of the colliding nucleus. So,  $A_{\text{part}} = -A_{\text{sp}} = N_{\text{spec,B}} - N_{\text{spec,F}}$ , where  $A_{\text{sp}}$  is the asymmetry between forward and backward moving spectators. By correlating  $A_{\text{ch},\eta}$  with  $A_{\text{sp}}$  on an event-by-event basis, we can quantify the

contribution of initial-state participant asymmetry to the rapidity-odd component of the longitudinal distribution of produced particles.

To reduce the detector effects, such as efficiency of spectator detection in experiments, the asymmetry variables are normalized as follows:

$$nA_{\text{sp}} = \frac{N_{\text{spec,F}} - N_{\text{spec,B}}}{N_{\text{spec,F}} + N_{\text{spec,B}}}, \quad nA_{\text{ch},\eta} = \frac{N_{\text{ch},\eta} - N_{\text{ch},-\eta}}{N_{\text{ch},\eta} + N_{\text{ch},-\eta}}. \quad (1)$$

The  $nA_{\text{sp}}$  is then correlated with  $nA_{\text{ch},\eta}$  using a modified Pearson correlation coefficient, denoted as  $\rho$ . Typically, the Pearson correlation coefficient is calculated by dividing the covariance  $\text{Cov}(nA_{\text{sp}}, nA_{\text{ch},\eta})$  by the square-root of the product of the variances of  $nA_{\text{sp}}$  and  $nA_{\text{ch},\eta}$ , referred to as  $\text{Var}(nA_{\text{sp}})$  and  $\text{Var}(nA_{\text{ch},\eta})$ , respectively. However, it is often necessary to employ modified versions of these variances in the definition of Pearson correlators to enhance the reliability of the measurements [53]. In the present study,  $nA_{\text{ch},\eta}$  is defined over a specific range of  $\delta\eta$ , such that  $N_{\text{ch},\eta} + N_{\text{ch},-\eta}$  is directly proportional to the width of  $\delta\eta$ . However, it is desirable to modify the definition of  $\text{Var}(nA_{\text{ch},\eta})$  such that it does not depend on definition of  $\delta\eta$ . With simple assumptions, we show that  $\text{Var}(nA_{\text{ch},\eta})$  is inversely proportional to  $\delta\eta$  (see Appendix). Therefore, to ensure that the measurement of  $\rho$  is independent of the choice of  $\delta\eta$ , we introduce a modified variance defined as  $\text{Var}(nA_{\text{ch},\eta})_{\text{mod}} = \text{Var}(nA_{\text{ch},\eta}) \cdot \delta\eta$ .

Hence, the modified form of Pearson correlator proposed in this study is:

$$\rho(nA_{\text{sp}}, nA_{\text{ch},\eta}) = -\frac{\text{Cov}(nA_{\text{sp}}, nA_{\text{ch},\eta})}{\sqrt{\text{Var}(nA_{\text{sp}})\text{Var}(nA_{\text{ch},\eta})_{\text{mod}}}}, \quad (2)$$

Over a large number of events in a given symmetric collision system, the mean of the distributions for  $nA_{\text{sp}}$  and  $nA_{\text{ch},\eta}$  approaches zero, implying that  $\text{Cov}(nA_{\text{sp}}, nA_{\text{ch},\eta}) \approx \langle nA_{\text{sp}} \cdot nA_{\text{ch},\eta} \rangle$ , and  $\text{Var}(nA_{\text{sp}}) \approx \langle (nA_{\text{sp}})^2 \rangle$ , where,  $\langle \rangle$  denotes averaging over an ensemble of events. In models that describe the distribution  $P(\eta)$ ,  $\text{Var}(nA_{\text{ch},\eta})_{\text{mod}}$  captures the fluctuations in the number of sources contributing to particle production at a given  $\eta$ . The negative sign used in Eq. 2 converts spectator asymmetry to participant asymmetry,  $nA_{\text{part}}$ , where, for a fixed  $N_{\text{part}}$ ,

$$nA_{\text{part}} = \frac{N_{\text{part,F}} - N_{\text{part,B}}}{N_{\text{part,F}} + N_{\text{part,B}}}, \quad nA_{\text{sp}} = -\frac{N_{\text{part}}}{N_{\text{spec}}} nA_{\text{part}}. \quad (3)$$

The form of  $\rho(nA_{\text{sp}}, nA_{\text{ch},\eta})$  offers significant advantages for experimental measurements. Traditionally, measurement of multiplicity correlations in experiments have been limited to the  $\eta$  range covered by tracking detectors which are positioned near mid-rapidity. However, in our study, the use of  $nA_{\text{ch},\eta}$  allows us to extend the measurement of the proposed correlator to relatively forward rapidities allowing the use of forward scintillators and calorimeters, which generate signals proportional to the number of tracks. In this context, any proportionality factor associated with these detectors cancels out to first order, thereby facilitating reliable measurements of the correlation coefficient across a broad  $\eta$  range. Furthermore, in different heavy-ion collision experiments, various detector subsystems in the central and forward  $\eta$  regions typically have different segmentation in  $\eta$ . By employing the modified variance  $\text{Var}(nA_{\text{ch}})_{\text{mod}}$ , it becomes feasible to consistently conduct measurement of the proposed correlator with different  $\delta\eta$  values, tailored to the choice of  $\delta\eta$  made for such measurements in respective detector subsystems. We will demonstrate later in this study that the measurements of both  $\text{Cov}(nA_{\text{sp}}, nA_{\text{ch},\eta})$  and  $\text{Var}(nA_{\text{ch}})_{\text{mod}}$  remain largely independent of the choice of  $\delta\eta$ .

The losses in number of detected spectators in forward and backward directions owing to spectator dynamics does not affect particle production near mid-rapidity. In other words, the space-time evolution of spectators is decoupled from that of the medium formed in relativistic heavy-ion collisions [31, 32]. Consequently, the spectator dynamics is not expected to contribute to  $\text{Cov}(nA_{\text{sp}}, nA_{\text{ch},\eta})$ . However, these dynamics increase the fluctuations measured by  $\text{Var}(nA_{\text{sp}})$ . So, the existence of spectator dynamics is expected to decrease the magnitude of the proposed correlator. The reduction in  $\rho(nA_{\text{sp}}, nA_{\text{ch},\eta})$  caused by spectator dynamics, compared to its magnitude in model scenarios where these processes are not considered, provides a strong constraint for modeling these processes. Therefore, in addition to the sensitivity to preferential emission,  $\rho(nA_{\text{sp}}, nA_{\text{ch},\eta})$  also captures the effect of spectator dynamics.

### 3. Results

We first examine the impact of preferential emission on  $P(\eta)$  by categorizing events based on  $A_{\text{sp}}$ , as shown in Figure 1(a). The events are divided into three categories: Region 1 for  $A_{\text{sp}} \ll 0$ , Region 2 for  $A_{\text{sp}} \approx 0$ , and Region 3

for  $A_{sp} \gg 0$ . Region 1 comprises events with a larger number of forward-going participants. According to preferential emission, particles produced from events in Region 1 are expected to predominantly populate large positive  $\eta$ , as seen in the  $P(\eta)$  distribution for these events in Figure 1(b).

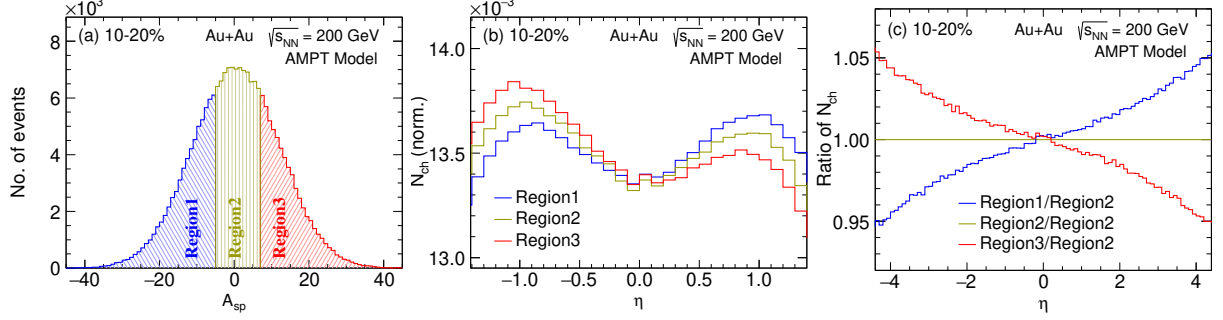


Figure 1: (a) Distribution of  $A_{sp}$  in 10–20% central Au+Au collisions at  $\sqrt{s_{NN}} = 200$  GeV. Regions 1, 2, and 3 denote events with  $A_{sp} \ll 0$ ,  $A_{sp} \approx 0$ , and  $A_{sp} \gg 0$ , respectively. (b) Comparison between  $\eta$  distribution of produced particles for events within Regions 1, 2, and 3. (c) Ratio between  $\eta$  distribution of produced particles for Region 1, Region 2, and Region 3 with respect to that of Region 3.

A comparison of  $P(\eta)$  ratios for events with  $A_{sp} \ll 0$  and  $A_{sp} \gg 0$  with respect to  $A_{sp} \approx 0$ , shown in Figure 1(c). The ratio reveals an excess of produced particles in the forward or backward  $\eta$  for events with more forward or backward moving participants, respectively. Thus, Figure 1 confirms that particle production via string fragmentation in the AMPT model agrees with expectations from preferential emission. The results presented in this study are limited to  $|\eta| \leq 4$ , which is sufficient to encompass the pseudorapidity coverage of the tracking detectors of all currently operating heavy-ion experiments.

We further quantify the effect of preferential emission on particle production using  $\rho(nA_{sp}, nA_{ch,\eta})$ , as shown in Figure 2. The observed correlation between  $nA_{sp}$ , and  $nA_{ch,\eta}$  suggests that the produced particles retain initial-state information about the participants' direction of motion. The rapidity-odd behavior of this correlator is evident from the observation:  $\rho(nA_{sp}, nA_{ch,\eta}) = -\rho(nA_{sp}, nA_{ch,-\eta})$ . For symmetric collisions, as  $\eta$  approaches zero,  $N_{ch,\eta} \approx N_{ch,-\eta}$  causing  $\rho(nA_{sp}, nA_{ch,\eta})$  to approach zero. The covariance and variances in the calculation of  $\rho(nA_{sp}, nA_{ch,\eta})$  are robust against statistical fluctuations arising from varying  $\delta\eta$  (see Appendix).

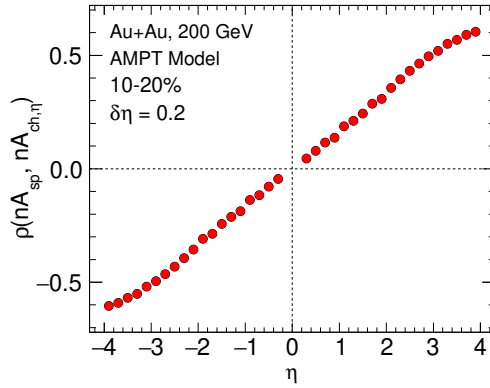


Figure 2:  $\rho(N_{spec,F}, N_{ch,\eta})$ ,  $\rho(nA_{sp}, nA_{ch,\eta})$  and  $\rho(nA_{sp}, nA_{ch,-\eta})$  for  $\delta\eta = 0.2$  in 10–20% central Au+Au collisions at  $\sqrt{s_{NN}} = 200$  GeV from the AMPT model.

Figure 3 shows  $Var(nA_{ch,\eta})_{mod}$ ,  $-Cov(nA_{sp}, nA_{ch,\eta})$ , and  $\rho(nA_{sp}, nA_{ch,\eta})$  as a function of  $\eta$  for different centralities. The  $Var(nA_{sp})$  is depicted as horizontal lines near  $\eta = 5.4$  corresponding to the beam rapidity for  $\sqrt{s_{NN}} = 200$  GeV [32] because it is an initial-state quantity and does not change with  $\eta$  within the AMPT model. The  $Var(nA_{ch,\eta})_{mod}$  gradually increases from mid- $\eta$  to forward- $\eta$ , reflecting a growing forward-backward asymmetry in number of produced particles, driven by an increased fluctuations in string endpoints [54, 22]. The magnitude of

$Cov(nA_{sp}, nA_{ch,\eta})$  also shows an increasing trend with  $\eta$ , indicating a stronger influence of initial-state asymmetry in  $N_{part}$  on the rapidity-odd component of  $P(\eta)$ . This observation is consistent with findings in Refs. [10, 44] using a different observable. The magnitude and trend of  $\rho(nA_{sp}, nA_{ch,\eta})$  provides similar information as  $Cov(nA_{sp}, nA_{ch,\eta})$ , but in a normalized form.

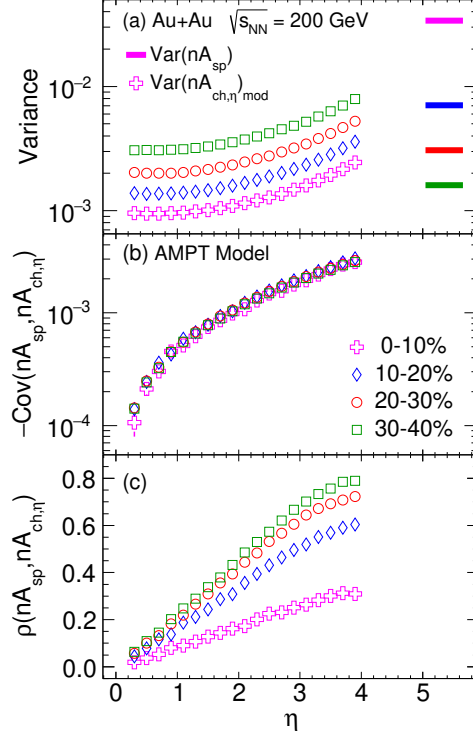


Figure 3: (a)  $Var(nA_{ch,\eta})_{mod}$ , (b)  $-Cov(nA_{sp}, nA_{ch,\eta})$ , and (c)  $\rho(nA_{sp}, nA_{ch,\eta})$  for different centralities as function of  $\eta$  in Au+Au collisions at  $\sqrt{s_{NN}} = 200$  GeV from the AMPT model.

As the collisions become increasingly central,  $Var(nA_{sp})$  is observed to increase as shown in Figure 3. This increase corresponds to decreasing  $Var(nA_{part})$ , following Eq. 3. The reduction in  $Var(nA_{part})$  reflects more equal numbers of forward and backward moving participants, leading to a production of more symmetric number of strings in both directions. Concurrently,  $Var(nA_{ch,\eta})_{mod}$  exhibits a decrease as collisions become more central indicating more symmetric particle production profile about  $\eta = 0$ . This implies the emergence of more longitudinally symmetric strings in relatively central collisions. The  $-Cov(nA_{sp}, nA_{ch,\eta})$  is shown in Figure 3(b) as a function of  $\eta$  for different centralities. The magnitude of the covariance only shows a small change with changing centrality. The centrality dependence of  $\rho(nA_{sp}, nA_{ch,\eta})$ , as shown in Figure 3(c), mainly stems from  $Var(nA_{sp})$ , reflecting fluctuations in the number of strings, and  $Var(nA_{ch,\eta})_{mod}$ , reflecting the longitudinal asymmetry of the strings.

However, only spectator neutrons are typically measured in experiments by ZDC detectors [25, 26, 55]. Therefore, to assess the sensitivity of the proposed correlator to spectator dynamics in a realistic experimental scenario, we compare the  $\rho(nA_{sp}, nA_{ch,\eta})$  measured with (1) neutron spectators ( $n_{spec}$ ) from the AMPT model, which lacks spectator dynamics, and, (2) free-neutron spectators detected by the ZDC after undergoing spectator dynamics referred to as “ $f_{spec}$ ” [32, 56]. The number of forward (backward) free-neutron spectators,  $f_{spec,F}$  ( $f_{spec,B}$ ) are estimated from experimental data using the method proposed in Ref. [10], briefly discussed here. The mean ( $\mu$ ) and width ( $\sigma$ ) of  $f_{spec}$  as function of  $N_{part}$  in Au+Au collisions at  $\sqrt{s_{NN}} = 200$  GeV were reported in Ref. [32], based on the PHENIX data [56]. The number of spectators in forward and backward directions are independent of each other [27]. Therefore, to independently sample  $f_{spec,F}$  and  $f_{spec,B}$ , both  $\mu$  and  $N_{part}$  (see Figure A.6 in Appendix) were reduced by a factor of 2, and  $\sigma$  was scaled down by  $\sqrt{2}$  to obtain the correlation between  $f_{spec,F}$  and  $N_{part,F}$ . Then, for a given  $N_{part,F}$  (and  $N_{part,B}$ ) in an AMPT event, the  $f_{spec,F}$  (and  $f_{spec,B}$ ) is sampled from a Gaussian distribution with mean  $\mu_f = \mu/2$  and

width  $\sigma_f = \sigma / \sqrt{2}$ . Finally, the proposed correlator, based on the estimated number of  $f_{\text{spec},F}$  and  $f_{\text{spec},B}$ , is calculated using Eq. 2.

Figure 4 presents a comparison of  $\rho(nA_{\text{sp}}, nA_{\text{ch},\eta})$  calculated using total spectators, neutron spectators, and free-neutron spectators. To assess the sensitivity to varying spectator dynamics reflected in  $\text{Var}(nA_{\text{sp}})$ , we include two scenarios with fluctuations of  $1\sigma_f$  and  $2\sigma_f$ . The magnitude of  $\rho(nA_{\text{sp}}, nA_{\text{ch},\eta})$  calculated using neutron spectators is observed to be smaller than the correlator calculated with total spectators by approximately 20% across all  $\eta$  and centralities (see Figure A.7 in Appendix). In contrast, a significant centrality dependence of  $\rho(nA_{\text{sp}}, nA_{\text{ch},\eta})$  for free-

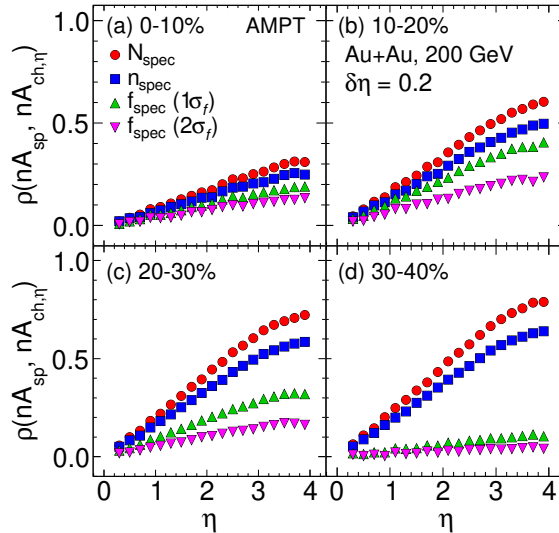


Figure 4: Comparison among  $\rho(nA_{\text{sp}}, nA_{\text{ch},\eta})$  calculated using total spectators ( $N_{\text{spec}}$ ), neutron spectators ( $n_{\text{spec}}$ ), and free-neutron spectators ( $f_{\text{spec}}$ ) for  $\delta\eta = 0.2$  in Au+Au collisions at  $\sqrt{s_{\text{NN}}} = 200$  GeV from the AMPT model. The  $1\sigma_f$  and  $2\sigma_f$  refer to two considered cases for different amount of fluctuations in  $f_{\text{spec}}$  owing to spectator dynamics.

neutron spectators, estimated from experimental data, is observed. In 0-10% central collisions, the correlation coefficient calculated using free-neutron spectators (with  $1\sigma_f$ ) is very close to that of neutron spectators. However, this value approaches zero for collisions in the 30 – 40% centrality range. Such a pronounced centrality dependence is attributed to increased spectator evaporation and fragmentation, as more spectators become available in relatively peripheral collisions. This finding is consistent with GEMINI model simulations, which indicate that the influence of spectator dynamics on  $f_{\text{spec}}$  increases as collisions become more peripheral [57]. Furthermore, the scenario with fluctuations of  $2\sigma_f$  leads to around 30 – 40% reduction in magnitude of  $\rho(nA_{\text{sp}}, nA_{\text{ch},\eta})$  compared to the scenario with fluctuation of  $1\sigma_f$ . Thus, the correlator is observed to display strong sensitivity to the fluctuations in number of spectators arising from spectator dynamics. Experimental measurement of  $\rho(nA_{\text{sp}}, nA_{\text{ch},\eta})$  would thus provide valuable understanding and strong constraints towards the dynamics governing spectator fragmentation and evaporation.

#### 4. Conclusion

Understanding the mechanisms governing the longitudinal distribution of particles in heavy-ion collisions, is essential for constraining initial state conditions and medium evolution. Traditionally, the rapidity-odd component of the  $\eta$  profile is constrained using asymmetric collision systems within model scenarios. In contrast, this study proposes a modified Pearson correlation coefficient between the initial-state asymmetry of  $N_{\text{spec}}$  and the  $\eta$ -asymmetry of  $N_{\text{ch}}$  in symmetric collisions systems. This approach quantifies the role of preferential emission towards the rapidity-odd component of  $\eta$  profile.

We illustrate the feasibility of this measurement in heavy-ion collision experiments using the AMPT model. Our findings demonstrate a strong correlation between the final-state longitudinal asymmetry of produced particles and the initial-state asymmetry between forward- and backward-moving participants. Notably, the magnitude of this correlation increases from mid- $\eta$  to forward  $\eta$ , consistent with expectations from preferential emission. Additionally, in

central collisions, we observe a smaller magnitude of the correlator, attributed to reduced forward-backward participant asymmetry and the consequent formation of more longitudinally symmetric strings.

The proposed correlator offers several unique advantages: Firstly, it relies solely on an inherent categorization of particle production sources into rapidity-odd and rapidity-even components, without imposing explicit assumptions about the particle production process. The observed rapidity-odd behavior emerges naturally from the particle production mechanisms within the model. Consequently, experimental measurements of this correlator can serve as a crucial test of the influence of preferential emission on particle distribution and related phenomena. Secondly, The formulation of the variables used in this correlator allows for consistent application across different detector subsystems, irrespective of their  $\eta$ -segmentation. This flexibility facilitates extending measurements into forward rapidities in experiments. Finally, the proposed correlator is highly sensitive to processes governing spectator matter evolution. Increased fluctuations in the number of spectators—due to evaporation and fragmentation—result in a reduced correlator magnitude. Thus, this correlator could effectively constrain these contributions, which are especially important at lower energies.

Thus, the novel observable  $\rho(nA_{\text{sp}}, nA_{\text{ch},\eta})$  offers a valuable tool for constraining the mechanisms governing the pseudorapidity distribution of produced particles and the space-time evolution of spectators in heavy-ion collisions. Future measurements of this correlator across different collision energies, particularly in the beam energy scan at RHIC, FAIR, and NICA experimental facilities would be valuable in elucidating these dynamics in heavy-ion collisions.

## Acknowledgements

The authors thank Subhasish Chattopadhyay, Jean-Yves Ollitrault, Govert Nijs, Victor Roy, Subhash Singha and Chunjian Zhang for their valuable comments. We also thank Elena Bratkovskaya for her insightful suggestions. SB is supported by U.S Department of Energy under grant number DEFG0287ER40331.

## Appendix A.

First, we justify the use of the modified variance  $Var(nA_{\text{ch},\eta})_{\text{mod}}$  in the proposed correlator. In this study, the distribution for  $N_{\text{ch},\eta}$  is calculated using particles within the pseudorapidity range of  $\eta \pm \frac{\delta\eta}{2}$ . To facilitate subsequent calculations, we express the normalized charged particle asymmetry as:

$$nA_{\text{ch},\eta} = \frac{N_{\text{ch},\eta} - N_{\text{ch},-\eta}}{N_{\text{ch},\eta} + N_{\text{ch},-\eta}} \equiv \frac{a}{b}, \quad (\text{A.1})$$

where  $a = N_{\text{ch},\eta} - N_{\text{ch},-\eta}$  and  $b = N_{\text{ch},\eta} + N_{\text{ch},-\eta}$ .

Next, we perform a Taylor expansion of  $nA_{\text{ch},\eta}$  to first order around the mean of  $a$  and  $b$ , denoted as  $\mu_a$  and  $\mu_b$ , respectively:

$$\begin{aligned} nA_{\text{ch},\eta} &= nA_{\text{ch},\eta}(\mu_a, \mu_b) + \left. \left( \frac{\partial nA_{\text{ch},\eta}}{\partial a} \right) \right|_{\mu_a, \mu_b} (a - \mu_a) + \left. \left( \frac{\partial nA_{\text{ch},\eta}}{\partial b} \right) \right|_{\mu_a, \mu_b} (b - \mu_b) \\ &= nA_{\text{ch},\eta}(\mu_a, \mu_b) + \frac{1}{\mu_b} (a - \mu_a) + \frac{\mu_a}{\mu_b^2} (b - \mu_b). \end{aligned} \quad (\text{A.2})$$

Now, we can approximate the variance of  $nA_{\text{ch},\eta}$ :

$$\begin{aligned} Var(nA_{\text{ch},\eta}) &\approx \left( \left. \frac{\partial nA_{\text{ch},\eta}}{\partial a} \right|_{\mu_a, \mu_b} \right)^2 Var(a) + \left( \left. \frac{\partial nA_{\text{ch},\eta}}{\partial b} \right|_{\mu_a, \mu_b} \right)^2 Var(b) \\ &= \frac{Var(a)}{\mu_b^2} + \frac{Var(b)\mu_a^2}{\mu_b^4}. \end{aligned} \quad (\text{A.3})$$

In the case of symmetric collisions, and in limit of a large number of events, we have  $\mu_a = 0$ . Assuming  $N_{\text{ch},\eta}$  and  $N_{\text{ch},-\eta}$  are independent,  $\text{Var}(a) = \text{Var}(b) = 2\text{Var}(N_{\text{ch},\eta})$  and  $\mu_b = 2\mu(N_{\text{ch},\eta})$ . Substituting these relationships yields:

$$\text{Var}(nA_{\text{ch},\eta}) \approx \frac{\sigma^2(N_{\text{ch},\eta})}{2\mu^2(N_{\text{ch},\eta})}. \quad (\text{A.4})$$

The expression thus obtained for  $\text{Var}(nA_{\text{ch},\eta})$ , defined within an infinitesimally small  $\delta\eta$ , can be denoted as  $\nu$ . Our objective is to investigate how  $\nu$  can be derived from measurements conducted within an arbitrarily large  $\delta\eta' = k\delta\eta$ , where  $k > 1$ .

Assuming uniform particle production in  $\eta$ , we can write:

$$\begin{aligned} \text{Var}(N_{\text{ch},\eta})_{k\delta\eta} &= k\text{Var}(N_{\text{ch},\eta})_{\delta\eta}, \\ \mu(N_{\text{ch},\eta})_{k\delta\eta} &= k\mu(N_{\text{ch},\eta})_{\delta\eta}. \end{aligned} \quad (\text{A.5})$$

Replacing in Eq. A.4, we obtain,

$$\begin{aligned} \text{Var}(nA_{\text{ch},\eta})_{\delta\eta'} &\approx \frac{\text{Var}(N_{\text{ch},\eta})_{\delta\eta}}{2k\mu^2(N_{\text{ch},\eta})_{\delta\eta}} = \frac{\nu}{k} = \frac{\nu\delta\eta}{\delta\eta'} \\ \text{Var}(nA_{\text{ch},\eta})_{\delta\eta'} \cdot \delta\eta' &= \text{Var}(nA_{\text{ch},\eta}) \cdot \delta\eta. \end{aligned} \quad (\text{A.6})$$

Thus,  $\text{Var}(nA_{\text{ch},\eta})_{\text{mod}} = \text{Var}(nA_{\text{ch},\eta})_{\delta\eta} \cdot \delta\eta$  is independent of changing  $\delta\eta$ .

This behavior is illustrated in Figure A.5, which highlights the sensitivity of the proposed correlator to changes in  $\delta\eta$ . The  $\text{Var}(nA_{\text{ch},\eta})_{\text{mod}}$ ,  $-\text{Cov}(nA_{\text{sp}}, nA_{\text{ch},\eta})$ , and  $\rho(nA_{\text{sp}}, nA_{\text{ch},\eta})$  are plotted as a function of  $\eta$  for different  $\delta\eta$  values. It can be clearly observed that within the assumptions made in defining  $\text{Var}(nA_{\text{ch},\eta})_{\text{mod}}$ , the variance, covariance, and correlator remain largely unchanged despite large variations in  $\delta\eta$ .

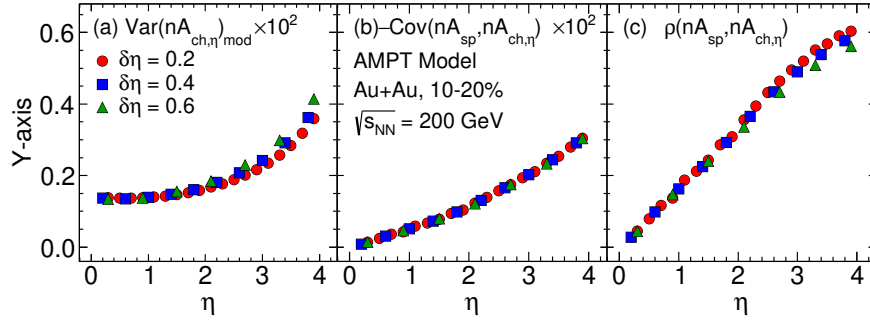


Figure A.5: (a)  $\text{Var}(nA_{\text{ch},\eta})_{\text{mod}}$ , (b)  $-\text{Cov}(nA_{\text{sp}}, nA_{\text{ch},\eta})$ , and (c)  $\rho(nA_{\text{sp}}, nA_{\text{ch},\eta})$  as a function of  $\eta$  for different  $\delta\eta$  in 10–20% central Au+Au collisions at  $\sqrt{s_{\text{NN}}} = 200$  GeV. The  $\text{Var}(nA_{\text{ch},\eta})_{\text{mod}}$  and  $-\text{Cov}(nA_{\text{sp}}, nA_{\text{ch},\eta})$  are arbitrarily scaled for better visibility.

Figure A.6(a) shows the estimated number of free-neutrons detected by the ZDC from the PHENIX experiment at RHIC versus the total number of participants. The 2D correlation is constructed using  $\mu$  and  $\sigma$  from the PHENIX data for Au+Au collisions at  $\sqrt{s_{\text{NN}}} = 200$  GeV [56], as reported in Ref. [32]. The number of forward-going spectators versus forward participants is then estimated from the correlation in panel (a), following the methodology proposed in Ref. [10], and briefly discussed in the paper, and is shown in panel (b) of Figure A.6.

Figure A.7 illustrates the impact of spectator dynamics on the proposed correlator. The figure presents the ratio of  $\rho(nA_{\text{sp}}, nA_{\text{ch},\eta})$  measured using total spectators ( $N_{\text{spec}}$ ) and free-neutron spectators ( $f_{\text{spec}}$ , adjusted for spectator dynamics) relative to neutron spectators ( $n_{\text{spec}}$ ) across four different centralities. The sensitivity to varying spectator dynamics is assessed by repeating measurement of  $\rho(nA_{\text{sp}}, nA_{\text{ch},\eta})$  with different fluctuation parameters  $1\sigma_f$  and  $2\sigma_f$ .

The  $\rho(nA_{\text{sp}}, nA_{\text{ch},\eta})$  calculated using  $n_{\text{spec}}$  consistently yields values approximately 20% smaller than those calculated with  $N_{\text{spec}}$ , regardless of centrality or  $\eta$ . However, the behavior observed with  $f_{\text{spec}}$  is noteworthy. For the case of  $1\sigma_f$ , the calculation of  $\rho(nA_{\text{sp}}, nA_{\text{ch},\eta})$  using  $f_{\text{spec}}$  agrees closely with that using  $n_{\text{spec}}$  in the 0-10% centrality, although this agreement deteriorates for more peripheral collisions. When the fluctuations in the number of spectators are increased to  $2\sigma_f$ , reflecting a greater contribution from spectator dynamics, a further reduction of approximately 40%

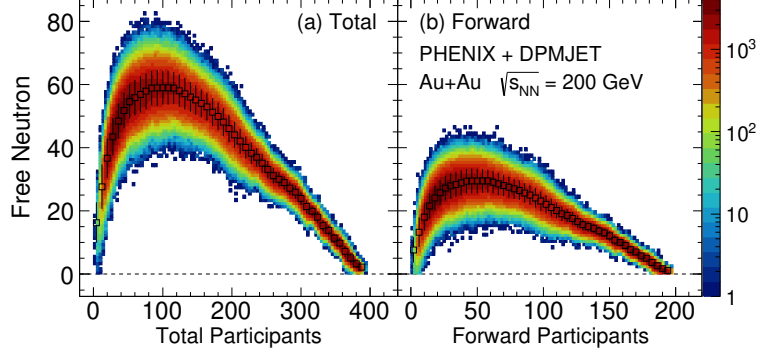


Figure A.6: (a)  $f_{\text{spec}}$  vs  $N_{\text{part}}$  for Au+Au collisions at  $\sqrt{s_{\text{NN}}} = 200$  GeV simulated using estimated mean and sigma of  $f_{\text{spec}}$  at given  $N_{\text{part}}$  in Ref. [32] using PHENIX data [56]. (b)  $f_{\text{spec},F}$  vs  $N_{\text{part},F}$  estimated using panel (a) following the methodology described in text. The respective mean and sigma values used are shown in black points and lines, respectively.

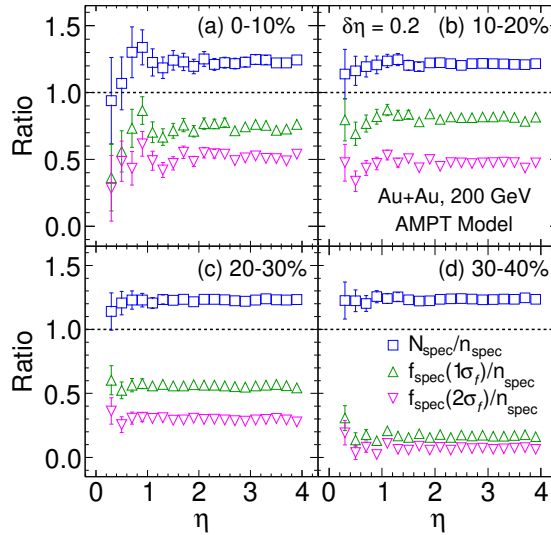


Figure A.7: Ratio between  $\rho(nA_{\text{sp}}, nA_{\text{ch},\eta})$  calculated using total spectators ( $N_{\text{spec}}$ ) and free-neutron spectators ( $f_{\text{spec}}$ ) in comparison to that calculated with neutron spectators ( $n_{\text{spec}}$ ) for  $\delta\eta = 0.2$  in Au+Au collisions at  $\sqrt{s_{\text{NN}}} = 200$  GeV. The  $1\sigma_f$  and  $2\sigma_f$  refer to two considered cases for different amount of fluctuations in  $f_{\text{spec}}$  owing to spectator dynamics.

is observed in the most central collisions. This indicates that the proposed correlator displays significant sensitivity to the influence of spectator dynamics simulated here by an increased fluctuations in number of detected spectators.

## References

- [1] M. Li, C. Shen, Longitudinal dynamics of high baryon density matter in high-energy heavy-ion collisions, *Phys. Rev. C* 98 (2018) 064908. [arXiv:1809.04034](#), [doi:10.1103/PhysRevC.98.064908](#).  
URL <https://link.aps.org/doi/10.1103/PhysRevC.98.064908>
- [2] L. Du, et al., Baryon transport and the qcd critical point, *Phys. Rev. C* 104 (2021) 064904. [arXiv:2107.02302](#), [doi:10.1103/PhysRevC.104.064904](#).  
URL <https://link.aps.org/doi/10.1103/PhysRevC.104.064904>
- [3] C. Shen, B. Schenke, Longitudinal dynamics and particle production in relativistic nuclear collisions, *Phys. Rev. C* 105 (2022) 064905. [arXiv:2203.04685](#), [doi:10.1103/PhysRevC.105.064905](#).  
URL <https://link.aps.org/doi/10.1103/PhysRevC.105.064905>
- [4] C. Shen, S. Alzhirani, Collision-geometry-based 3d initial condition for relativistic heavy-ion collisions, *Phys. Rev. C* 102 (2020) 014909. [arXiv:2003.05852](#), [doi:10.1103/PhysRevC.102.014909](#).  
URL <https://link.aps.org/doi/10.1103/PhysRevC.102.014909>
- [5] L. Du, et al., Probing initial baryon stopping and equation of state with rapidity-dependent directed flow of identified particles, *Phys. Rev. C* 108 (2023) L041901. [arXiv:2211.16408](#), [doi:10.1103/PhysRevC.108.L041901](#).  
URL <https://link.aps.org/doi/10.1103/PhysRevC.108.L041901>
- [6] J. Jia, P. Huo, A method for studying the rapidity fluctuation and decorrelation of harmonic flow in heavy-ion collisions, *Phys. Rev. C* 90 (3) (2014) 034905. [arXiv:1402.6680](#), [doi:10.1103/PhysRevC.90.034905](#).
- [7] J. Jia, et al., Observables for longitudinal flow correlations in heavy-ion collisions, *J. Phys. G* 44 (7) (2017) 075106. [arXiv:1701.02183](#), [doi:10.1088/1361-6471/aa74c3](#).
- [8] M. Aaboud, et al., Measurement of longitudinal flow decorrelations in Pb+Pb collisions at  $\sqrt{s_{NN}} = 2.76$  and 5.02 TeV with the ATLAS detector, *Eur. Phys. J. C* 78 (2) (2018) 142. [arXiv:1709.02301](#), [doi:10.1140/epjc/s10052-018-5605-7](#).
- [9] G. Aad, et al., Longitudinal Flow Decorrelations in Xe+Xe Collisions at  $\sqrt{s_{NN}} = 5.44$  TeV with the ATLAS Detector, *Phys. Rev. Lett.* 126 (12) (2021) 122301. [arXiv:2001.04201](#), [doi:10.1103/PhysRevLett.126.122301](#).
- [10] J. Jia, et al., Forward-backward multiplicity fluctuation and longitudinal harmonics in high-energy nuclear collisions, *Phys. Rev. C* 93 (4) (2016) 044905. [arXiv:1506.03496](#), [doi:10.1103/PhysRevC.93.044905](#).
- [11] G. Aad, et al., Forward-backward correlations and charged-particle azimuthal distributions in pp interactions using the ATLAS detector, *JHEP* 07 (2012) 019. [arXiv:1203.3100](#), [doi:10.1007/JHEP07\(2012\)019](#).
- [12] M. Gazdzicki, M. I. Gorenstein, Transparency, mixing and reflection of initial flows in relativistic nuclear collisions, *Phys. Lett. B* 640 (2006) 155–161. [arXiv:hep-ph/0511058](#), [doi:10.1016/j.physletb.2006.07.044](#).
- [13] M. Gyulassy, X.-N. Wang, HIJING 1.0: A Monte Carlo program for parton and particle production in high-energy hadronic and nuclear collisions, *Comput. Phys. Commun.* 83 (1994) 307. [arXiv:nuc1-th/9502021](#), [doi:10.1016/0010-4655\(94\)90057-4](#).
- [14] Z.-W. Lin, et al., A Multi-phase transport model for relativistic heavy ion collisions, *Phys. Rev. C* 72 (2005) 064901. [arXiv:nuc1-th/0411110](#), [doi:10.1103/PhysRevC.72.064901](#).
- [15] S. Ferreres-Solé, T. Sjöstrand, The space-time structure of hadronization in the Lund model, *Eur. Phys. J. C* 78 (11) (2018) 983. [arXiv:1808.04619](#), [doi:10.1140/epjc/s10052-018-6459-8](#).
- [16] M. Rohrmoser, W. Broniowski, Forward-backward multiplicity fluctuations in ultrarelativistic nuclear collisions with wounded quarks and fluctuating strings, *Phys. Rev. C* 99 (2) (2019) 024904. [arXiv:1809.08666](#), [doi:10.1103/PhysRevC.99.024904](#).
- [17] W. Broniowski, M. Rohrmoser, Correlations with fluctuating strings, *Acta Phys. Polon. B* 50 (2019) 1019. [arXiv:1904.06955](#), [doi:10.5506/APhysPo1B.50.1019](#).
- [18] A. Bialas, W. Czyz, Wounded nucleon model and Deuteron-Gold collisions at RHIC, *Acta Phys. Polon. B* 36 (2005) 905–918. [arXiv:hep-ph/0410265](#).
- [19] A. Bzdak, Forward-backward multiplicity correlations in the wounded nucleon model, *Phys. Rev. C* 80 (2009) 024906. [arXiv:0902.2639](#), [doi:10.1103/PhysRevC.80.024906](#).
- [20] A. Bzdak, K. Wozniak, Forward-backward multiplicity fluctuations in heavy nuclei collisions in the wounded nucleon model, *Phys. Rev. C* 81 (2010) 034908. [arXiv:0911.4696](#), [doi:10.1103/PhysRevC.81.034908](#).
- [21] P. Bozek, I. Wyskiel, Directed flow in ultrarelativistic heavy-ion collisions, *Phys. Rev. C* 81 (2010) 054902. [arXiv:1002.4999](#), [doi:10.1103/PhysRevC.81.054902](#).
- [22] P. Bozek, W. Broniowski, The torque effect and fluctuations of entropy deposition in rapidity in ultra-relativistic nuclear collisions, *Phys. Lett. B* 752 (2016) 206–211. [arXiv:1506.02817](#), [doi:10.1016/j.physletb.2015.11.054](#).
- [23] L.-G. Pang, et al., Decorrelation of anisotropic flow along the longitudinal direction, *Eur. Phys. J. A* 52 (4) (2016) 97. [arXiv:1511.04131](#), [doi:10.1140/epja/i2016-16097-x](#).
- [24] M. Rohrmoser, W. Broniowski, Longitudinal correlations from fluctuating strings in Pb-Pb, p-Pb, and p-p collisions, *Phys. Rev. C* 101 (1) (2020) 014907. [arXiv:1909.01702](#), [doi:10.1103/PhysRevC.101.014907](#).
- [25] G. Dellacasa, et al., ALICE technical design report of the zero degree calorimeter (ZDC)<https://cds.cern.ch/record/381433> (3 1999).
- [26] R. Arnaldi, et al., The Zero degree calorimeters for the ALICE experiment, *Nucl. Instrum. Meth. A* 581 (2007) 397–401, [Erratum: *Nucl. Instrum. Meth. A* 604, 765 (2009)]. [doi:10.1016/j.nima.2008.04.009](#).
- [27] R. Staszewski, et al., Forward proton detectors in heavy ion physics, *Acta Phys. Polon. B* 50 (2019) 1229. [arXiv:1903.09498](#), [doi:10.5506/APhysPo1B.50.1229](#).
- [28] J. J. Chwastowski, et al., Probing Geometry of Ion-Ion Collisions with Roman Pot Detectors (11 2020). [arXiv:2011.00872](#).

- [29] J. J. Gaimard, K. H. Schmidt, A Reexamination of the abrasion - ablation model for the description of the nuclear fragmentation reaction, Nucl. Phys. A 531 (1991) 709–745. doi:10.1016/0375-9474(91)90748-U.
- [30] J. Hufner, et al., Abrasion-ablation in reactions between relativistic heavy ions, Phys. Rev. C 12 (1975) 1888–1898. doi:10.1103/PhysRevC.12.1888.
- [31] B. B. Back, et al., Participant and spectator scaling of spectator fragments in Au+Au and Cu+Cu collisions at  $\sqrt{s_{NN}} = 19.6$  and 22.4 GeV, Phys. Rev. C 94 (2) (2016) 024903. arXiv:1511.07921, doi:10.1103/PhysRevC.94.024903.
- [32] S. Tarafdar, et al., A Centrality Detector Concept, Nucl. Instrum. Meth. A 768 (2014) 170–178. arXiv:1405.4555, doi:10.1016/j.nima.2014.09.060.
- [33] B. Alver, et al., Phobos results on charged particle multiplicity and pseudorapidity distributions in Au+Au, Cu+Cu, d+Au, and p+p collisions at ultra-relativistic energies, Phys. Rev. C 83 (2011) 024913. arXiv:1011.1940, doi:10.1103/PhysRevC.83.024913.
- [34] A. Sorensen, et al., Dense nuclear matter equation of state from heavy-ion collisions, Prog. Part. Nucl. Phys. 134 (2024) 104080. arXiv:2301.13253, doi:10.1016/j.ppnp.2023.104080.
- [35] L. Zheng, E. C. Aschenauer, J. H. Lee, Determination of electron-nucleus collision geometry with forward neutrons, Eur. Phys. J. A 50 (12) (2014) 189. arXiv:1407.8055, doi:10.1140/epja/i2014-14189-3.
- [36] L. Shi, Transport phenomena in heavy-ion reactions, Ph.D. thesis, Michigan State U. (2003). doi:10.25335/M5804XW0W.
- [37] H. Appelshäuser, et al., Spectator nucleons in Pb + Pb collisions at 158-A-GeV, Eur. Phys. J. A 2 (1998) 383–390. doi:10.1007/s100500050135.
- [38] L. Adamczyk, et al., Beam-Energy Dependence of the Directed Flow of Protons, Antiprotons, and Pions in Au+Au Collisions, Phys. Rev. Lett. 112 (16) (2014) 162301. arXiv:1401.3043, doi:10.1103/PhysRevLett.112.162301.
- [39] P. Bozek, et al., Torqued fireballs in relativistic heavy-ion collisions, Phys. Rev. C 83 (2011) 034911. arXiv:1011.3354, doi:10.1103/PhysRevC.83.034911.
- [40] W. Broniowski, P. Bozek, Longitudinal correlations in the initial stages of ultra-relativistic nuclear collisions, EPJ Web Conf. 141 (2017) 05003. arXiv:1610.09673, doi:10.1051/epjconf/201714105003.
- [41] A. Bialas, A. Bzdak, Wounded quarks and diquarks in high energy collisions, Phys. Rev. C 77 (2008) 034908. arXiv:0707.3720, doi:10.1103/PhysRevC.77.034908.
- [42] A. Bzdak, Measurement of asymmetric component in proton-proton collisions, Acta Phys. Polon. B 41 (2010) 151. arXiv:0904.0869.
- [43] B. Kellers, G. Wolschin, Limiting fragmentation at LHC energies, PTEP 2019 (5) (2019) 053D03. arXiv:1901.06421, doi:10.1093/ptep/ptz044.
- [44] J. Jia, Forward-backward multiplicity correlations in pp, p + Pb and Pb + Pb collisions with the ATLAS detector, Nucl. Phys. A 956 (2016) 405–408. arXiv:1601.01296, doi:10.1016/j.nuclphysa.2016.02.044.
- [45] J. Jia, et al., Separating the Impact of Nuclear Skin and Nuclear Deformation in High-Energy Isobar Collisions, Phys. Rev. Lett. 131 (2) (2023) 022301. arXiv:2206.10449, doi:10.1103/PhysRevLett.131.022301.
- [46] J. Xu, C. M. Ko, Higher-order anisotropic flows and dihadron correlations in Pb-Pb collisions at  $\sqrt{s_{NN}} = 2.76$  TeV in a multiphase transport model, Phys. Rev. C 84 (2011) 044907. arXiv:1108.0717, doi:10.1103/PhysRevC.84.044907.
- [47] J. Xu, C. M. Ko, Triangular flow in heavy ion collisions in a multiphase transport model, Phys. Rev. C 84 (2011) 014903. arXiv:1103.5187, doi:10.1103/PhysRevC.84.014903.
- [48] D. Solanki, et al., Beam energy dependence of Elliptic and Triangular flow with the AMPT model, Phys. Lett. B 720 (2013) 352–357. arXiv:1210.0512, doi:10.1016/j.physletb.2013.02.028.
- [49] J. Jia, et al., Precision Tests of the Nonlinear Mode Coupling of Anisotropic Flow via High-Energy Collisions of Isobars, Chin. Phys. Lett. 40 (4) (2023) 042501. arXiv:2206.07184, doi:10.1088/0256-307X/40/4/042501.
- [50] E. G. Nielsen, Y. Zhou, Transverse momentum decorrelation of the flow vector in Pb–Pb collisions at  $\sqrt{s_{NN}} = 5.02$  TeV, Eur. Phys. J. C 83 (6) (2023) 545. arXiv:2211.13651, doi:10.1140/epjc/s10052-023-11693-7.
- [51] N. Magdy, et al., Investigation of the Elliptic Flow Fluctuations of the Identified Particles Using the a Multi-Phase Transport Model, Universe 6 (9) (2020) 146. arXiv:2009.02734, doi:10.3390/universe6090146.
- [52] Z.-W. Lin, L. Zheng, Further developments of a multi-phase transport model for relativistic nuclear collisions, Nucl. Sci. Tech. 32 (10) (2021) 113. arXiv:2110.02989, doi:10.1007/s41365-021-00944-5.
- [53] S. A. Voloshin, Heavy ion collisions: Correlations and fluctuations in particle production, J. Phys. Conf. Ser. 50 (2006) 111–118. arXiv:nucl-ex/0505003, doi:10.1088/1742-6596/50/1/013.
- [54] X.-Y. Wu, L.-G. Pang, G.-Y. Qin, X.-N. Wang, Longitudinal fluctuations and decorrelations of anisotropic flows at energies available at the CERN Large Hadron Collider and at the BNL Relativistic Heavy Ion Collider, Phys. Rev. C 98 (2) (2018) 024913. arXiv:1805.03762, doi:10.1103/PhysRevC.98.024913.
- [55] Y.-F. Xu, et al., Physics performance of the STAR zero degree calorimeter at relativistic heavy ion collider, Nucl. Sci. Tech. 27 (6) (2016) 126. doi:10.1007/s41365-016-0129-z.
- [56] S. S. Adler, et al., Systematic studies of the centrality and  $\sqrt{s_{NN}}$  dependence of the  $d E(T) / d \eta$  and  $d (N(\text{ch}) / d \eta)$  in heavy ion collisions at mid-rapidity, Phys. Rev. C 71 (2005) 034908, [Erratum: Phys. Rev. C 71, 049901 (2005)]. arXiv:nucl-ex/0409015, doi:10.1103/PhysRevC.71.034908.
- [57] L.-M. Liu, et al., Probing neutron-skin thickness with free spectator neutrons in ultracentral high-energy isobaric collisions, Phys. Lett. B 834 (2022) 137441. arXiv:2203.09924, doi:10.1016/j.physletb.2022.137441.